# Particle Motion Induced by Bubble Cavitation

Stéphane Poulain,[1] Gabriel Guenoun,[2] Sean Gart,[3] William Crowe,[3] and Sunghwan Jung[3,*]
[1]Université de Toulouse, ISAE-Supaero, Département Aérodynamique, Énergétique et Propulsion, 10 avenue Edouard Belin, 31400 Toulouse, France
[2]Department of Physics, ENS Cachan, 61 Avenue du Président Wilson, 94230 Cachan, France
[3]Department of Biomedical Engineering and Mechanics, Virginia Tech, Blacksburg, Virginia 24061, USA
(Received 28 February 2015; published 27 May 2015)

Cavitation bubbles induce impulsive forces on surrounding substrates, particles, or surfaces. Even though cavitation is a traditional topic in fluid mechanics, current understanding and studies do not capture the effect of cavitation on suspended objects in fluids. In the present work, the dynamics of a spherical particle due to a cavitation bubble is experimentally characterized and compared with an analytical model. Three phases are observed: the growth of the bubble where the particle is pushed away, its collapse where the particle approaches the bubble, and a longer time scale postcollapse where the particle continues to move toward the collapsed bubble. The particle motion in the longer time scale presumably results from the asymmetric cavitation evolution at an earlier time. Our theory considering the asymmetric bubble dynamics shows that the particle velocity strongly depends on the distance from the bubble as an inverse-fourth-power law, which is in good agreement with our experimentation. This study sheds light on how small free particles respond to cavitation bubbles in fluids.

DOI: 10.1103/PhysRevLett.114.214501 PACS numbers: 47.55.dp, 47.55.N−, 47.55.dd

Cavitation is the physical process of bubble formation in a liquid medium by either decreasing pressure or increasing temperature. These cavitation bubbles are well known for causing undesirable damage in hydrodynamic systems [1] and offer advantages in many other systems, e.g., in sonocatalytic reactors [2], in noninvasive fracturing tools of kidney stones [3,4], and in drug delivery methods [5]. They are also present in natural systems: inside the human body [6], used as a hunting technique of some crustaceans [7,8], in plants [9], or in everyday life [10].

During the cavitation mechanism, a vapor bubble is nucleated and is rapidly turned back to its equilibrium liquid phase [11]. The detailed dynamics of spherical bubbles far from any boundaries, described by the Rayleigh-Plesset equation, has been extensively studied [12,13]. Most experimental configurations of interest are a cavitated bubble occurring near either solid or deformable boundaries [14–18] and a stationary bubble near moving particles [19,20]. For biomedical and engineering applications, the effect of ultrasonic cavitation on deformations or fracture of large biotissue or bioagglomerate [3–5,21] and on collisions of micrometric particles [22] have been studied. However, cavitation in the vicinity of freely moving objects has received less attention, and little is known about how a particle responds to a cavitation bubble of similar size.

In this present work, we propose an experimental study of the interaction between a cavitation bubble and a freely moving particle whose radius is smaller than the maximum bubble radius. We identify the response of the particle to the bubble dynamics, and also develop an analytical model for the particle behavior after the disappearance of the bubble that is compared with our experimental data.

There are two ways to initiate cavitation in water according to its phase diagram [23]: by lowering the pressure or by raising the temperature. In practice, pressure-based mechanisms are widely used due to their relatively simple setups [24]; however, with these methods it is difficult to precisely control the cavitation bubble's location. As an alternative method, superheated cavitation bubbles are generated by laser pulses [25] or by electric sparks [26,27], and it is more convenient to control and study a single bubble and its effects [28–30]. We have chosen the spark-induced approach in this study. The electric spark is generated by the discharge of capacitors (the equivalent capacitance of the circuit is 23.5 mF) that can be charged up to 50 V. Two tinned copper electrodes linked to the circuit, approximately 0.17 mm in diameter, are touched together at the desired location of the nucleation. A trigger initiates the discharge of the capacitors, creating a short circuit and thereby a spark that nucleates a cavitation bubble. Experiments are performed in a Plexiglas tank filled with filtered water at room temperature. The bubble is nucleated far enough from the tank walls and from the air-water surface to neglect the effects of these boundaries. Three different voltages are used to charge the capacitors: 40, 45, and 50 V. Below 40 V no significant movement of the particles has been observed. This nucleates bubbles with respective maximal radii of $R_{b,\max} = 2.6 \pm 0.1$, $3.3 \pm 0.2$, and $3.9 \pm 0.2$ mm; growing times $t_g = 0.45 \pm 0.03$, $0.58 \pm 0.06$, and $0.68 \pm 0.08$ ms; and

 

collapsing times $t_c = 0.31 \pm 0.04$, $0.42 \pm 0.07$, and $0.51 \pm 0.08$ ms.

The cavitation is initiated near a single solid spherical particle attached to a thin steel rod whose radius and mass are $R_{\text{rod}} = 0.2$ mm and $m_{\text{rod}} = 0.07$ g, which hangs under gravity like a pendulum with a free rotation. Hence, the bending of the rod is not considered and has not been observed in our experiments ($N = 241$). The nucleation point and the center of the particle are positioned on a horizontal line, making the motion of the latter one dimensional: considering the small horizontal displacements analyzed, less than 1 mm, and the length of the rod, $l_{\text{rod}} \sim 65$ mm, it is assumed that vertical displacements are negligible. The motion of the particle is hence only characterized by the distance from its center to the nucleation point, designated by $X_p(t)$. Six different particles are used: three glass particles, whose radii $R_p$ are 2.4, 2.0, and 1.6 mm, and three other 1.6 mm particles made of aluminium, brass, and steel. Their masses $m_p$ are, respectively, 0.14, 0.08, 0.04, 0.05, 0.14, and 0.13 g.

The motion of the particle and the evolution of the bubble are recorded with a Photron FASTCAM Mini high-speed camera, with 12 500 to 64 000 frames/s depending of the need of spatial and temporal resolution. The particle position is tracked using MATLAB codes. A sample image sequence is shown in Fig. 1. Dynamics of the bubble and the particle can be divided into the following three phases, illustrated by Fig. 2. (i) Just after the electric spark, the cavitation bubble grows and pushes the particle away ($\dot{X}_p > 0$) until it reaches its maximal size. (ii) The bubble then starts to collapse in on itself, sucking the particle toward its center ($\dot{X}_p < 0$). The bubble evolution is qualitatively similar to what has already been reported for a cavitation bubble near a fixed rigid convex surface [31]: it grows almost spherically, but takes a characteristic shape during the collapse as seen Fig. 1(d). (iii) Once the bubble has collapsed [see Fig. 1(e)], it rebounds and collapses again several times. The rebounds become progressively smaller, and then the bubble finally disappears. During this time, the particle continues to move toward the center of the bubble as illustrated in Fig. 1(f).

We studied the particle during the last phase of suction in which, as shown Fig. 2(b), it has a constant speed, denoted by $\dot{X}_{p,f}$, for a long time compared to the time scale of the bubble dynamics. An analytical theory has been developed to evaluate the effect of the particle properties, the initial distance $X_{p,i}$ from the nucleation point, and the bubble dynamics. The evolution of the bubble creates a flow in which the fluid velocity $\boldsymbol{u}$ is found from the incompressibility of the fluid [33]: using spherical coordinates centered at the nucleation site, the velocity is radial, $\boldsymbol{u} = u\boldsymbol{e_r}$ with

$$u(r,t) = \left(\frac{R_b(t)}{r}\right)^2 \dot{R}_b(t), \tag{1}$$

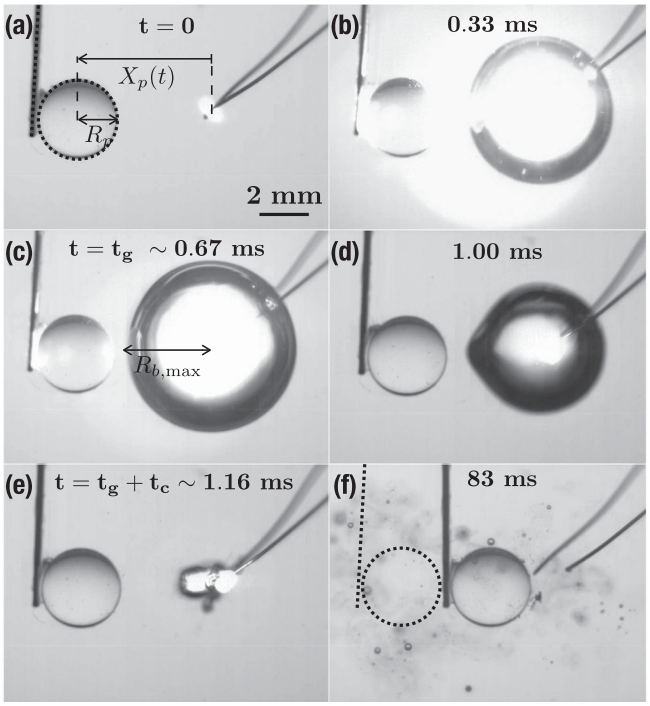


FIG. 1. Image sequences of a glass particle (left), 1.6 mm in radius, and a cavitation bubble (right). A 50 V spark (a) nucleates a cavitation bubble that begins to expand, (b) pushing the particle away. The bubble then reaches its maximum size (c) and begins to attenuate in volume. As it shrinks, it is no longer able to maintain its spherical shape (d) and will collapse in on itself to its nucleation point (e). The collapse of the cavitation bubble sucks the particle toward the nucleation site (f). In all of the images, the time represents the time since the electric spark. For details, see the Supplemental Material [32].

where $R_b$ is the bubble radius. An important geometric parameter for bubble dynamics near boundaries is the stand-off parameter $\gamma = (X_{p,i} - R_p)/R_{b,\max}$, the ratio of the initial distance between the solid boundary and the bubble center to the maximum bubble radius [34]. In our experiments, we only consider $\gamma > 1$. The drag force on the particle due to the flow is $\boldsymbol{F}_{\text{drag}} = F_{\text{drag}}(t)\boldsymbol{e_r}$ with

$$F_{\text{drag}}(t) = \text{sgn}(u)\frac{1}{2}C_D\rho_w A[u(X_p(t),t)]^2, \tag{2}$$

where $A = \pi R_p^2$ is the projected area of the particle, $\rho_w$ is the density of water, and $C_D$ is the drag coefficient taken as a constant.

The particle and the rod form a pendulum system that follows the angular momentum equation $I\ddot{\theta} = -l_{\text{rod}}F_{\text{drag}}$, where $I$ is the moment of inertia of the system around its axis of rotation. With small angular displacements $\theta$ [$\theta = (X_{p,i} - X_p)/l_{\text{rod}}$] and particles much smaller than the rod length ($R_p/l_{\text{rod}} \ll 1$), the angular momentum equation becomes $m_{\text{eff}}\ddot{X}_p = F_{\text{drag}}$, with $m_{\text{eff}} = m_{\text{rod}}/3 + m_p + \rho_w\pi(R_{\text{rod}}^2 l_{\text{rod}} + 2R_p^3)/3$ where the last term accounts

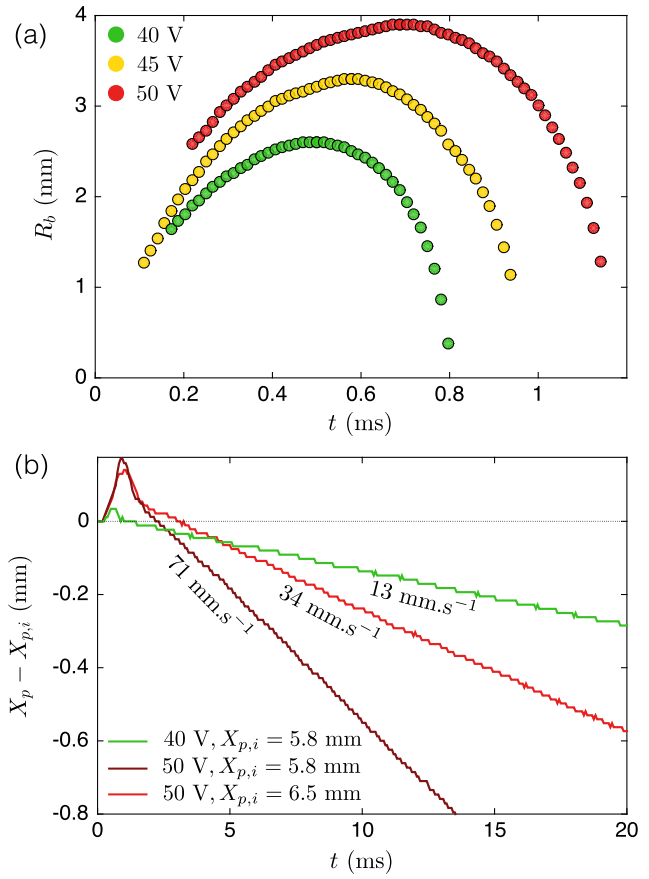


FIG. 2 (color online). (a) Evolution of the bubble radius generated by 40, 45, and 50 V sparks, measured without the presence of a particle. Because of the initial spark, the bubble radius is unmeasurable at the very beginning of the growth. (b) Displacement of a brass particle with a radius of 1.6 mm due to cavitation, showing the strong dependence on the initial distance and the bubble dynamics. The measured final velocity is given for each case.

for the added mass of rod and particle. The velocity of the particle can be evaluated by integrating this equation of motion over the first two phases. For simplicity, the particle displacement during the growth and the collapse of the bubble is neglected: in the drag expression, Eq. (2), we assume $X_p = X_{p,i}$. This approximation is experimentally justified: the particle position was measured in our experiments during these phases, giving a maximum departure from the initial position $\Delta X_{p,i}/X_{p,i} \sim 0.3$–$5\%$. Therefore, we obtain

$$\dot{X}_{p,f} = \frac{\frac{1}{2} C_D \rho_w \pi R_p^2}{X_{p,i}^4 m_{\text{eff}}} \left( \int_0^{t_g} R_b^4 \dot{R}_b^2 dt - \int_{t_g}^{t_g+t_c} R_b^4 \dot{R}_b^2 dt \right), \tag{3}$$

where $t_g$ and $t_c$ are, respectively, the duration of the growing and collapsing phase of the bubble. We assume that the bubble follows the same form of evolution during

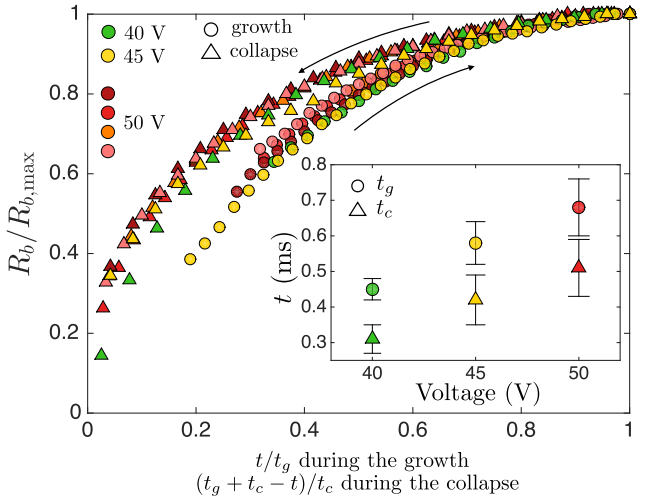


FIG. 3 (color online). Normalized bubble radius vs normalized growing or collapsing times. Circles correspond to the growing phase of the bubble, triangles to the collapsing phase. The inset shows the growth time and the collapse time for the different voltages.

the growth and the collapse, i.e., a self-similar solution $f$ such as

$$\frac{R_b(t)}{R_{b,\max}} = \begin{cases} f\left(\frac{t}{t_g}\right) & \text{if } t \in [0; t_g] \\ f\left(\frac{t_g+t_c-t}{t_c}\right) & \text{if } t \in [t_g; t_g + t_c]. \end{cases} \tag{4}$$

This self-similar approximation is motivated by the fact that the collapse of an empty spherical bubble follows a similar scaling [35]. Figure 3 shows the bubble radius in the growing and collapsing phases in order to verify the self-similar approximation. The growing phase is shown to be slightly slower than the collapsing phase in the normalized scales. This discrepancy might be due to a fact that the beginning of the spark is not necessarily the nucleation moment ($t = 0$) of cavitation as used in current measurements. Hence, the real $t_g$ could be shorter than the one we plotted in Fig. 3, which shifts the data points up and left closer to the curve in the collapsing phase. The slight mismatch between the approximation and experimental measurements is presumably attributed to the experimental difficulty in measuring the nucleation time. Still, it is verified *a posteriori* that the deviation is small enough to give a good scaling.

Using Eq. (4), the integral term in Eq. (3) becomes $-\int_0^1 f^4 f'^2 \times R_{b,\max}^6/\tau$, where $\tau = t_g t_c/(t_g - t_c)$ is a characteristic time of the bubble. This characteristic time is always positive because the collapse is faster than the growth, and $\tau$ can be seen as a measure of the asymmetry of the bubble evolution. From these results, the dimensionless velocity and position are defined, respectively, as $\dot{X}^*_{p,f} = -\dot{X}_{p,f} \times m_{\text{eff}}\tau/(\rho_w R_p^2 R_{b,\max}^2)$ and $X^*_{p,i} = X_{p,i}/R_{b,\max}$, leading to the following power-law relation:

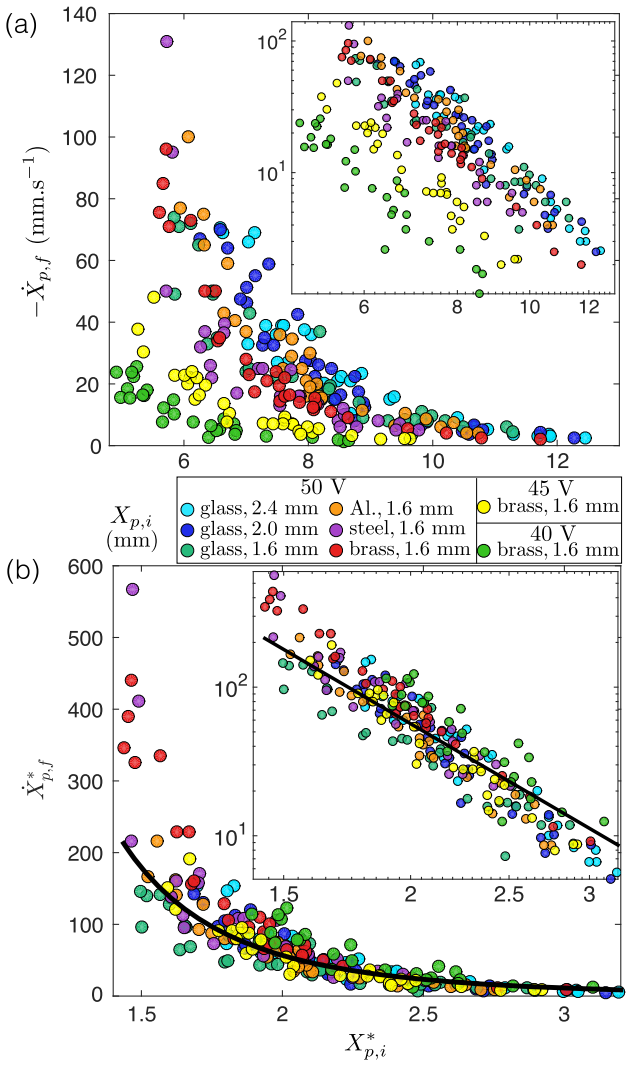


FIG. 4 (color online). (a) Velocity of the particle vs initial distance. (b) Normalized particle velocity vs normalized distance. Data with six different particles are used with a bubble generated by a 50 V spark, and one of the particles is also analyzed with 40 and 45 V sparks. The solid line represents a power law of −4, which is predicted in Eq. (5).

$$\dot{X}^*_{p,f} \propto (X^*_{p,i})^{-4}. \tag{5}$$

Figure 4(a) shows the particle velocity as a function of the distance with three different particle sizes, four different materials, and three different voltages. By normalizing the velocity and the distance based on the above analytical theory, we find that experimental data collapse well into Eq. (5) as shown in Fig. 4(b).

In conclusion, we observed and characterized the effect of a spark-induced cavitation bubble on a distant and small tethered spherical particle. This present study focuses on the final phase of the coupled dynamics, where the particle continues to move toward the center of the bubble because of the asymmetric bubble dynamics. The particle velocity inversely depends on the density and radius of the particle, and approximately on the fourth power of the initial distance from the bubble.

Our analytical theory is under the assumption of spherical bubbles and is then only valid for large $\gamma$ values. We even observed that when the spark occurs very close to the particle, the particle can go away from the bubble because of the strong influence of the rebound. Nevertheless, the inverse-fourth-power law is close to the experimental results with $\gamma > 1$, even though it underestimates the effect of the distance (the best-fit slope on our data is $-4.8 \pm 0.4$). As the bubble is cavitated near the particle, some deviations from the prediction have also been observed: heavier particles (brass and steel) move faster than expected compared to light particles (glass). In future work, we plan on investigating the detailed consequence of the precise bubble dynamics on the particle response, especially for $\gamma$ values close to and less than 1.

The authors acknowledge support from the National Science Foundation (CBET-1336038) and the Virginia Tech Institute for Critical Technology and Applied Science. Also, the authors thank Dr. J. Hanna for the loan of the high-speed camera.

*sunnyjsh@vt.edu

[1] A. Karimi and J. L. Martin, Int. Met. Rev. **31**, 1 (1986).
[2] T. J. Mason, *Sonochemistry: The Uses of Ultrasound in Chemistry* (The Royal Society of Chemistry, London, 1990).
[3] N. L. Miller and J. E. Lingeman, Br. Med. J. **334**, 468 (2007).
[4] J. Lingeman, J. McAteer, E. Gnessin, and A. Evanm, Nat. Rev. Urol. **6**, 660 (2009).
[5] C. Coussios and R. Roy, Annu. Rev. Fluid Mech. **40**, 395 (2008).
[6] A. Unsworth, D. Dowson, and V. Wright, Ann. Rheum. Dis. **30**, 348 (1971).
[7] M. Versluis, B. Schmitz, A. von der Heydt, and D. Lohse, Science **289**, 2114 (2000).
[8] S. N. Patek, W. L. Korff, and R. L. Caldwell, Nature (London) **428**, 819 (2004).
[9] A. Stroock, V. Pagay, M. Zwieniecki, and N. Michele Holbrook, Annu. Rev. Fluid Mech. **46**, 615 (2014).
[10] J. Rodriguez-Rodriguez, A. Casado-Chacon, and D. Fuster, Phys. Rev. Lett. **113**, 214501 (2014).
[11] D. Oxtoby, J. Phys. Condens. Matter **4**, 7627 (1992).
[12] C. Brennen, *Cavitation and Bubble Dynamics* (Oxford University Press, New York, 1995).
[13] P. Debenedetti, *Metastable Liquids: Concepts and Principles* (Princeton University Press, Princeton, 1996).
[14] J. R. Blake and D. C. Gibson, Annu. Rev. Fluid Mech. **19**, 99 (1987).
[15] E. Brujan, K. Nahen, P. Schmidt, and A. Vogel, J. Fluid Mech. **433**, 251 (2001).
[16] O. Lindau and W. Lauterborn, J. Fluid Mech. **479**, 327 (2003).

[17] P. Prentice, A. Cuschieri, K. Dholakia, M. Prausnitz, and P. Campbell, Nat. Phys. **1**, 107 (2005).
[18] E.-A. Brujan, K. Nahen, P. Schmidt, and A. Vogel, J. Fluid Mech. **433**, 251 (2001).
[19] R. R. Dagastine, G. B. Webber, R. Manica, G. W. Stevens, F. Grieser, and D. Y. C. Chan, Langmuir **26**, 11921 (2010).
[20] G. B. Webber, R. Manica, S. A. Edwards, S. L. Carnie, G. W. Stevens, F. Grieser, R. R. Dagastine, and D. Y. C. Chan, J. Phys. Chem. C **112**, 567 (2008).
[21] S. Zhu, F. H. Cocks, G. M. Preminger, and P. Zhong, Ultrasound Med. Biol. **28**, 661 (2002).
[22] T. Prozorov, R. Prozorov, and K. S. Suslick, J. Am. Chem. Soc. **126**, 13890 (2004).
[23] F. Caupin and E. Herbet, C.R. Phys. **7**, 1000 (2006).
[24] T. Leighton, *The Acoustic Bubble* (Academic Press, New York, 1997).
[25] L. Mart-Lpez, R. Ocaa, J. Porro, M. Morales, and J. Ocaa, Appl. Opt. **48**, 3671 (2009).
[26] C. Kling and F. Hammitt, J. Fluids Eng. **94**, 825 (1972).
[27] B. Karri, S. R. G. Avila, Y. C. Loke, S. J. O'Shea, E. Klaseboer, B. C. Khoo, and C.-D. Ohl, Phys. Rev. E **85**, 015303 (2012).
[28] W. Song, M. Hong, B. Lukyanchuk, and T. Chong, J. Appl. Phys. **95**, 2952 (2004).
[29] C.-D. Ohl, M. Arora, R. Dijkink, V. Janve, and D. Lohse, Appl. Phys. Lett. **89**, 074102 (2006).
[30] T. Sato, M. Tinguely, M. Oizumi, and M. Farhat, Appl. Phys. Lett. **102**, 074105 (2013).
[31] Y. Tomita, P. B. Robinson, R. P. Tong, and J. R. Blake, J. Fluid Mech. **466**, 259 (2002).
[32] See Supplemental Material at http://link.aps.org/supplemental/10.1103/PhysRevLett.114.214501 for high-speed movies showing the effect of a cavitation bubble on a particle.
[33] M. S. Plesset and A. Prosperetti, Annu. Rev. Fluid Mech. **9**, 145 (1977).
[34] Y. Tomita and A. Shima, J. Fluid Mech. **169**, 535 (1986).
[35] D. Obreschkow, M. Bruderer, and M. Farhat, Phys. Rev. E **85**, 066303 (2012).